Conf-901208--15

Behavior of Liquid Metal Droplets in an Aspirating Nozzle

EGG-M--90412

DE92 017846

W. D. Swank
J. R. Fincke
T. A. Mason

Idaho National Engineering Laboratory
EG&G Idaho, Inc.
Idaho Falls, ID 83415-2211

ABSTRACT -- Measurements of particle size, velocity, and relative mass flux were made on a spray field produced by aspirating liquid tin into 350° C argon flowing through a venturi nozzle via a small orifice in the throat of the nozzle. Details of the aspiration and droplet formation process were observed through windows in the nozzle. The spatial distribution of droplet size, velocity, and relative number density were measured at a location 10 mm from the nozzle exit. Due to the presence of separated flow in the nozzle, changes in nozzle inlet pressure did not significantly effect resulting droplet size and velocity. This suggests that good aerodynamic nozzle design is required if spray characteristics are to be controlled by nozzle flow.

NOMENCLATURE

ρ_l = Density of liquid metal

ρ_g = Density of gas

V = Relative velocity between the gas and the liquid

μ_l = Dynamic viscosity of liquid metal

σ = Surface tension of liquid metal

d = Droplet diameter

We = Weber number $\rho_g V^2 d/\sigma$

On = Ohnesorge number $\mu_l/(\rho_l d\sigma)^{1/2}$

INTRODUCTION

Spray forming is the sequential process of liquid metal atomization and droplet consolidation onto a substrate. The process examined here is the aspiration of liquid metal through orifices located in the throat of a venturi nozzle. Subsequent interaction with the gas stream breaks up the liquid metal into small droplets. After exiting the nozzle the droplets impact a substrate to form the product. Studies have shown [1,2] that spray deposited materials have microstructural features that greatly enhance the mechanical properties of the material, namely, fine uniformly sized, homogeneous, equiaxed grains. The microstructure of the deposit depends to a great extent on the conditions of the droplets prior to impact.

The break up of liquid droplets in a gas stream is a complex process consisting of mechanical and fluid dynamic phenomenon. Four modes of breakup have been observed in previous studies and are well defined in the literature.[3] The driving force in all four modes is the velocity differential between the gas and the droplet. This relative velocity produces an aerodynamic force proportional to $\rho_g V^2$. The four modes identified are,

1. vibrational or rotational breakup,
2. bag breakup,
3. shear or stripping breakup, and
4. chaotic breakup.

The vibrational form of breakup occurs when a relatively large liquid globule is stretched by the flowing gas or its own rotational inertia and oscillation of the elongated shape develops at its natural frequency. If conditions are right the

amplitude of these oscillations can increase until the drop breaks up. Bag breakup occurs when a droplet presents a flattened or slightly concave surface to the gas flow. The pressure differential across the droplet causes the center to be blown out into a bag shape which grows until it bursts, producing droplets of a smaller size. The stripping mode of breakup is observed at higher relative velocities. The gas flowing over the front surface of the droplet induces motion in the liquid toward the downstream side of the droplet. When this shearing force is higher than the resisting force of the surface tension, the drop loses mass in the form of thin sheets, filaments, or droplets. The final mode of breakup is termed chaotic. In this mode the droplet has been observed to shatter almost immediately into a cloud of relatively small droplets due to the extremely high relative velocities.

The purpose of this work was to begin to characterize the size and velocity of the droplets produced, and to investigate the details of the liquid metal breakup and droplet formation in the spraying process. Experimentally the particle size was determined from the absolute magnitude of scattered laser light, simultaneously the particle velocity was measured using a crossed beam laser Doppler velocimeter (LDV). In addition the relative mass flux is determined by measuring the accumulated thickness of tin on a substrate. Flow visualization using a strobed video technique and schlieren photography were also performed.

EXPERIMENTAL METHOD

A schematic of the experimental set up is shown in Figure 1. The converging diverging nozzle under investigation here was two dimensional. Only the vertical dimensions varied with axial location in the nozzle while the span

wise dimension was held constant. The throat to exit area ratio was 1:13 with a total included exit angle of 18°. A single alumina aspiration tube extends from the throat of the nozzle down into the electrically heated crucible below. The ratio of aspiration tube flow area to nozzle throat area was 1:20. The spray apparatus operates as follows, argon gas flows through a flow control valve and into the electrical resistance type heater. Upon exiting the heater the gas is at the desired temperature of 350° C and enters the converging section of the spray nozzle where it is accelerated. The nozzle was operated in the subsonic regime and therefore the gas reaches it's highest velocity, but it's lowest static pressure in the throat of the nozzle. Molten tin at 600° C is aspirated from the crucible below when the pressure differential between the static pressure in the throat of the nozzle and the pressure at the bottom of the aspiration tube (approximately atmospheric pressure), is great enough to over come the surface tension forces and liquid metal static head in the aspiration tube. Once in the throat of the nozzle the liquid metal is entrained into the gas and accelerated. Both exit the nozzle to impact the substrate.

The nozzle was constructed as a sandwich of three layers. The middle layer was fabricated from boron nitride and forms the floor and ceiling of the converging, throat and diverging sections. The outer layers form the walls of the nozzle and are machined from 6061 aluminum. Borosilicate windows are held in place against the boron nitride by the outer aluminum layers. The inside surface of the windows is flush with the nozzle side walls. A graphite type gasket seals the windows and makes up the seals between the aluminum and boron nitride layers of the nozzle. The windows provide optical access to the throat and diverging sections of the nozzle.

Optical access was required for the schlieren and video flow visualization

techniques. The schlieren system used the expanded beam of a 10 milliwatt helium-neon laser to characterize shock wave structure in the gas flow. Density gradients in the nozzle refract the collimated laser light as it passes through the nozzle. Next, a simple lens collects this light and forms an image of the test section. A knife edge is positioned at the focal point of this lens in such a manner as to eliminate the refracted light. This results in light and dark regions at the image caused by the gradients in gas density. These gradients are indications of shock wave structure. A strobed video technique was employed to visualize the aspiration and subsequent droplet formation process. This technique uses a strobe light synchronized to a CCD video camera. The camera is coupled to a 100 mm long focal length reflecting microscope. Although the standard frame rate (60 Hz) of the video camera did not allow us to follow the trajectory of a single particle in flight, the short duration of the strobe, 4 to 5 μsec, produced sharp images of the droplets.

The system developed for simultaneous measurement of particle size and velocity integrates a crossed beam laser Doppler velocimeter (LDV) with a scattered light particle size measurement. A schematic of the measurement system optics appears in Figure 2. The beam launching optics consist of two Brewster angle dispersing prisms that separate the individual colors in a multi-line 6 W argon ion laser beam. The blue 488 nm beam is routed, via a 1500 mm focal length lens and aperture/beam stop, to the measurement volume by a series of mirrors. The green 514 nm beam is routed to the LDV optics. These optics consist of a polarization rotator, a beam splitter, a beam expander and a 600 mm focal length focusing lens. The system is aligned such that the LDV measurement volume (0.173 x 4.2 mm) is located in the center of the large (2 mm) blue sizing beam. The effective length of the LDV measurement volume is further shortened to

approximately 0.75 mm by an aperture, P1, in the receiving optics. Localization of the LDV measurement volume in the center of the sizing beam and the requirement of coincidence between a particle size signal and a Doppler burst avoids the trajectory ambiguity problem of large particles clipping the periphery of the sizing beam and producing a signal representative of a smaller particle.

The receiving optics are also shown schematically in Figure 2. Lens L_1 (f = 350 mm) is placed one focal length away from the measurement volume. Lens L_2 (f = 250 mm) forms the de-magnified (1:0.71) image of the measurement volume on a 0.5 mm aperture P_1. The image of P_1 is transferred to the faces of detectors 1 and 2. The laser light scattered from the particle is collected at 90° to the axis of the beams and is directed to the sizing and velocimetry detectors through laser line filters (1 nm FWHM) centered at 488 and 514 nm, respectively.

The current pulse produced in the photomultipliers upon observation of a particle is converted to a voltage pulse by 50 ohm input, DC-150 Mhz response, pulse amplifiers. A counter-type signal processor is used to derive velocity data from individual Doppler bursts. The first positive cycle of the Doppler burst gates a programmable clock that controls two digitizers. A system controller and 128K memory module complete the CAMAC format data acquisition system. Once the programmable clock is triggered a predetermined number of samples (generally twenty) are recorded by the individual digitizers. The sample rate is set according to the general characteristics of the waveforms as determined by particle velocity. After acquisition of a predetermined number of particle waveforms the data are transferred to a microcomputer for subsequent processing. Data processing includes consistency checks to determine if valid data on size and velocity channels exist at the same temporal location in the

recorded waveform. The data are converted to engineering units using calibration factors determined prior to testing.

CALIBRATION AND MEASUREMENT UNCERTAINTY

Calibration of the particle size measurement system is performed against a Berglund-Liu vibrating orifice aerosol generator using methanol as the working fluid. A correction to this calibration, based on Mie scattering theory and published values of the material's index of refraction, is then generated. Finally, the calibration is checked against actual particles. The major sources of uncertainty are in the calibration standard and fit of the calibration coefficients, and random and long term drift in the photo detectors. These lead to an estimated one standard deviation in the measured diameter of 4.9 μm.

In calibrating the laser Doppler velocimeter only the laser wavelength and the angle between the beams are required to establish the relationship between the velocity of the scattering particle and the frequency output of the photodetector. The accuracy of the counter processor is checked against a standard function generator. The estimated velocity uncertainty is less than 5%.

RESULTS

FLOW VISUALIZATION - Schlieren photography produced evidence of strong density gradients, i.e. shock waves, in the throat and divergent sections of the nozzle. When the upstream pressure in the nozzle is increased to approximately twice atmospheric pressure, the velocity in the throat is sonic and a standing normal shock wave is formed at the exit of the throat. As the upstream pressure is increased, the flow separates from the floor of the nozzle and the normal shock blows out of the throat region, evolving into an oblique shock structure attached

to the ceiling of the nozzle. Under these conditions the gas velocity at the exit of the nozzle is subsonic and the flow profile inside the nozzle consists of a high velocity jet near the ceiling of the nozzle and a low velocity or recirculating eddy at the floor of the nozzle. This case is illustrated in the schematic and schlieren photograph of Figure 3. The undesirable flow separation is due to the relatively large included angle of the diverging section and is not unexpected. If a uniformly filled flow channel and supersonic velocities are desired, proper nozzle geometry and symmetry are required.

Figure 4 is a photograph of liquid tin being aspirated into the flow of the venturi throat and subsequently breaking up. Strobed video recordings, at a slightly higher magnification than the still photograph, were made for the purpose of studying the liquid metal behavior inside the nozzle. Due to the standard 60 Hz video field rate, it was not possible to follow the flight of a single particle. However, it could be seen that as tin is aspirated into the throat region, relatively large cylindrical (approximately 300 μm diameter X 900 μm long) globules are lofted into the flow stream. These globules are further elongated and broken up into several fragments, in a form of the vibrational and rotational mode of breakup. Between the larger droplet fragments are smaller satellite droplets, which are on the order of 30 μm in diameter. The larger droplet fragments deform again, and this process continues until the surface tension forces in the small droplets are larger than or equal to the forces produced by the difference in velocity between the droplets and the gas. Further downstream, aerodynamic forces are still greater than the surface tension of some larger droplets and evidence of bag breakup has been observed. It was also observed that the breakup process is complete within 10 to 15 mm downstream of the throat. Other liquid metal droplet breakup investigations [4] have observed

similar particle formation processes.

PARTICLE SIZE AND VELOCITY MEASUREMENTS - Particle size and velocity were measured at a location 10 mm downstream of the nozzle exit. Figure 5 is a typical particle size distribution taken on the centerline. The nozzle inlet pressure was 168 kPa with the argon at a temperature of 350° C and the tin melt temperature at 600° C. The average particle diameter calculated as an arithmetic mean based on a length scale is 28 μm. This suggests that 28 μm is the surface tension/ aerodynamic force balance limit for particle breakup. The appearance of some larger particles indicates that it is possible for droplets to survive acceleration long enough to reach the point where the aerodynamic forces are no longer great enough to cause breakup. Also shown in Figure 5 is the distribution on a mass fraction basis. Less than 10% of the mass, for these spray conditions, is made up of particles smaller than 28 μm in diameter. If a narrower distribution of size is desirable, i.e. more complete breakup, the liquid metal must remain in a region of high velocity gas flow for a longer period of time.

Exhausting to an atmospheric pressure of 85.5 Kpa (approx. 1500 m above sea level) the nozzle is choked at an inlet pressure of approximately 170 kPa. At pressures greater than this critical pressure supersonic flow would be expected in the divergent section of the nozzle. However, due to the geometry of the nozzle under investigation, separation of the flow initiates in the throat and the flow immediately shocks down to subsonic velocities. Therefore, the maximum gas velocity in the nozzle is very close to the calculated sonic velocity of 430 m/s and varies only slightly between an inlet pressure of 155 and 210 kPa. Although the velocity of the gas does not change the density of the gas does increase by 34% over this range of inlet pressures. Since the aerodynamic force

on the droplets is proportional to $\rho_g V^2$, this increase in density of the gas may explain the variation in average measured particle size towards smaller particles at higher nozzle inlet pressures shown in Figure 6. The data points shown in Figure 6 are an arithmetic mean of all the particle size measurements made at the 10 mm stand off distance with a tin melt temperature of 600°C.

The Weber number (We) is the dimensionless parameter most often encountered when discussing droplet break-up. It represents the ratio of aerodynamic forces of the gas to the surface tension forces of the liquid droplet.

$$We = \frac{\rho_g V^2 d}{\sigma}$$

The critical value of Weber number is defined as the We for which the aerodynamic forces are less than or equal to the surface tension forces. At the critical We the droplet no longer breaks up due to aerodynamic forces. Using the average particle diameter of 28 μm corresponding to the conditions of Figure 5, an average critical We was calculated to be approximately 9. The critical Weber number is generally considered to be a function of Ohnesorge number, which is a dimensionless parameter dependent on liquid properties only. It may be considered physically as the ratio of viscous forces, to the product of the inertial and surface tension forces in the droplet.

$$On = \frac{\mu_l}{(\rho_l d \sigma)^{1/2}}$$

Values of On tend to be small for liquid metals (low viscosity and high surface tension). The On for a tin droplet 28 μm in diameter at 600°C is equal to $4 \cdot 10^{-3}$.

The present Weber number of 9 is in good agreement with the data compiled by Pilch and Erdman [5] of critical Weber number data as a function of Ohnesorge number from a variety of authors.

Figure 7 shows the vertical distribution of average particle size at a stand off distance of 10 mm from the nozzle exit. Again the nozzle inlet pressure was 168 kPa with the argon at a temperature of 350° C and the tin melt temperature at 600° C. The plot shows that the smaller particles tend to migrate to the outer edges of the flow and that the larger particles stay on the center line. Thus, for a substrate passed vertically in front of this nozzle, the larger particles would be preferentially deposited in the middle of the sprayed layer. The maximum particle mass flux also occurs near the centerline of the nozzle, as shown in Figure 8. This data was obtained for the same conditions as Figure 7, but at a stand off distance of 75 mm. A substrate was placed in the spray and once sufficient tin had accumulated on the substrate it was sectioned. The thickness of the deposit was measured along the section to give an indication of the relative mass flux. The larger size of the particles and greater particle mass flux, hence energy flux, at the center of the spray will lower the cooling rate of the middle portion of the deposit. This has the potential to affect the distribution of grain structure in the deposit and possibly the mechanical properties of the product.

A typical distribution of particle velocities is shown in Figure 9 for a center line location 10 mm from the exit of the nozzle and the same spray conditions of Figure 5. The average particle velocity is 39 m/s with a standard deviation of 6 m/s. This is a narrow range of particle velocities, indicating that large and small droplets are accelerated to very nearly the same velocity. Due to the separation of the gas flow and the resulting recirculation zone, one

would expect the particles in the upper region of the field to be traveling at a higher velocity. Only slight indications of this are shown in the vertical spatial distribution of velocity, Figure 10. A simple one-dimensional model shows that particles in this size range reach 80% of their maximum velocity 6 mm downstream of the throat. Therefore, nearly all of the droplet acceleration takes place in the first few millimeters of the throat/divergent section of the nozzle and in this case the velocity field downstream of the throat has very little influence on the particle velocity at the exit of the nozzle. As the nozzle inlet pressure was varied for a tin melt temperature of 600°C, no significant differences in average particle velocity were detected at a stand off distance of 10 mm, Figure 11. Again, this result is explained by the slight variation in gas velocity in the throat region of the nozzle for choked flow followed by flow separation.

CONCLUSIONS

The geometry of the venturi nozzle under investigation here produced separated flow between inlet pressures of 155 and 210 kPa. When flow separation is present the gas flow does not go supersonic in the diverging section, but instead shocks down to subsonic velocities and decelerates in the divergent section of the nozzle. Under these conditions the highest gas velocity is the sonic velocity occurring in the nozzle throat region. Changing the inlet pressure over the range investigated does not change the gas velocity significantly. Consequently the high differential velocity between droplet and gas exists only in the throat and first few millimeters down stream of the throat. It was observed through video flow visualization that most of the droplet breakup occurs during acceleration in the throat and immediately downstream of the throat, where aerodynamic forces are greatest. The plots of

average particle size and velocity versus nozzle inlet pressure show very little change over the range of inlet pressures investigated. Therefore, with a nozzle geometry which produces separated flow resulting in operation only in the subsonic regime, there is limited ability to control the resulting particle size and velocity through nozzle inlet pressure.

The estimated Weber number for a nozzle inlet pressure of 168 kPa, a tin melt temperature of 600°C and an average droplet diameter of 28 μm is 9, which matches well with previous data at similar Ohnesorge numbers. From the same data it was also observed that a high percentage of the mass flux is made up of relatively large droplets which survived acceleration. If a narrower distribution of droplet diameters is desirable, a well designed nozzle without separation is required. The presence of supersonic gas velocities will result in a greater time/distance for the liquid metal to experience high aerodynamic forces resulting in more complete droplet breakup.

There are other controllable process parameters which have not been fully investigated. Examples are, liquid metal super heat (affecting surface tension and viscosity), aspiration hole size (affecting primary droplet size), and nozzle geometry. The combination of flow visualization, flow field characterization, and particle parameter measurements can provide insight into the physics of the aspirated spray process. This understanding, coupled with studies of product characteristics will ultimately lead to optimization and better control of the spray forming process.

ACKNOWLEDGEMENT

This work was supported by the U.S. Department of Energy, under DOE Contract No. DE-AC07-76ID01570.

REFERENCES

1. A.R.E. Singer and R.W. Evans, "Incremental Solidification and Forming", Metals Technology, 1983, Vol. 10, 61-68.

2. E.J. Lavernia and N.J. Grant, "Structures and Properties of a Modified 7075 Aluminum Alloy Produced by Liquid Dynamic Compaction", Internat. J. Rapid Solidification, 1986, Vol. 2, 93-106.

3. R. E. Luna and W. A. Klikoff, Jr., "On Aerodynamic Breakup of Liquid Drops", SC-RR-66-2716, Sandia Laboratory, Albuquerque, June 1967.

4. A. Unal, "Production of Rapidly Solidified Aluminum Alloy Powders by Gas Atomization and their Applications", Powder Metallurgy, 1990, Vol. 33, No. 1.

5. M. Pilch and C. A. Erdman, "Use of Breakup Time Data and Velocity History Data to Predict the Maximum Size of Stable Fragments for Acceleration-Induced Breakup of a Liquid Drop", Internat. J. Multiphase Flow, Vol. 13, No. 6, PP. 741-757, 1987.

Figure 1 - Schematic of spraying apparatus.

Figure 2 - Schematic of beam transmission and receiving optics indicating paths of the laser Dopler velocimeter, size measurement laser beams and collected scattered light.

Figure 3 - (a) Schlieren photograph of oblique shock waves and (b) schematic representation of separated flow in the nozzle.

Figure 4 - Breakup of liquid tin in the throat region of the nozzle.

Figure 5 - Size distribution of tin particles measured in flight 10 mm from the exit of the nozzle.

Figure 6 - Average droplet diameter as a function of nozzle inlet pressure measured 10 mm from the exit of the nozzle.

Figure 7 - Vertical spatial distribution of average droplet diameter at 10 mm from the exit of the nozzle.

Figure 8 - Relative mass flux in the spray field.

Figure 9 - Velocity distribution of particles measured in flight 10 mm from the exit of the nozzle.

Figure 10 - Vertical spatial distribution of average particle velocity at 10 mm from the exit of the nozzle.

Figure 11 - Average particle velocity as a function of nozzle inlet pressure measured 10 mm from the exit of the nozzle.

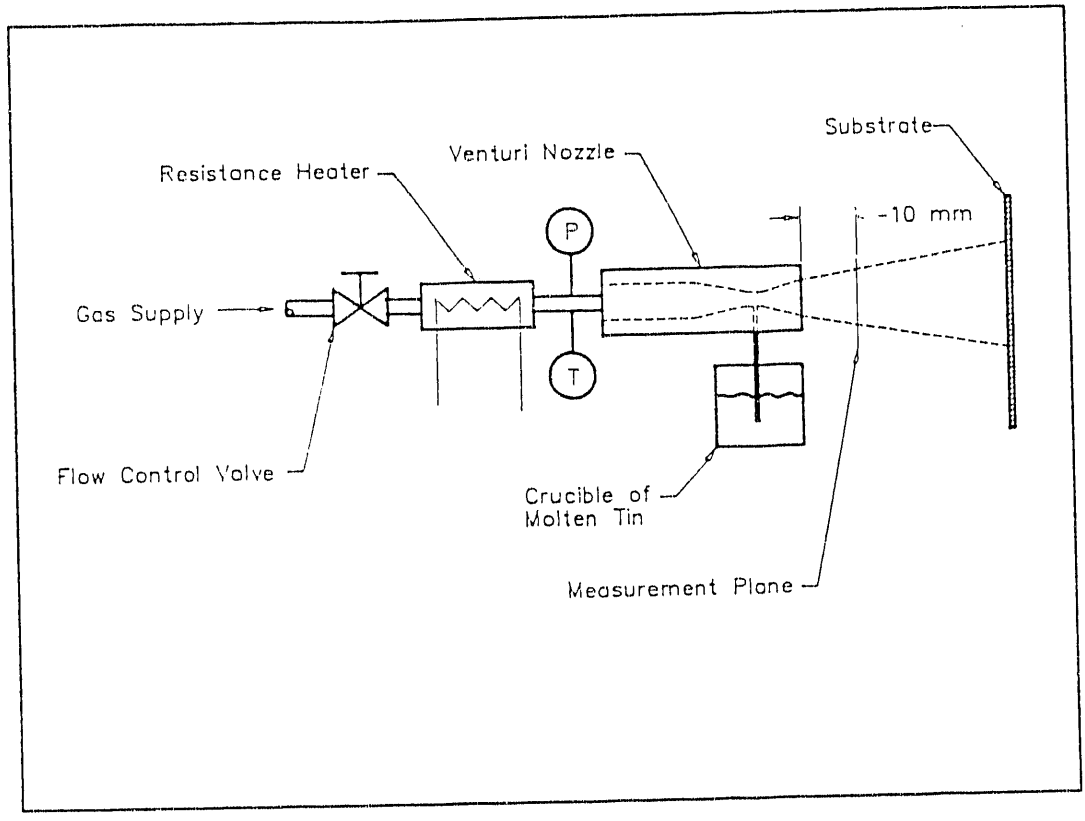

Figure 1 - Schematic of spraying apparatus.

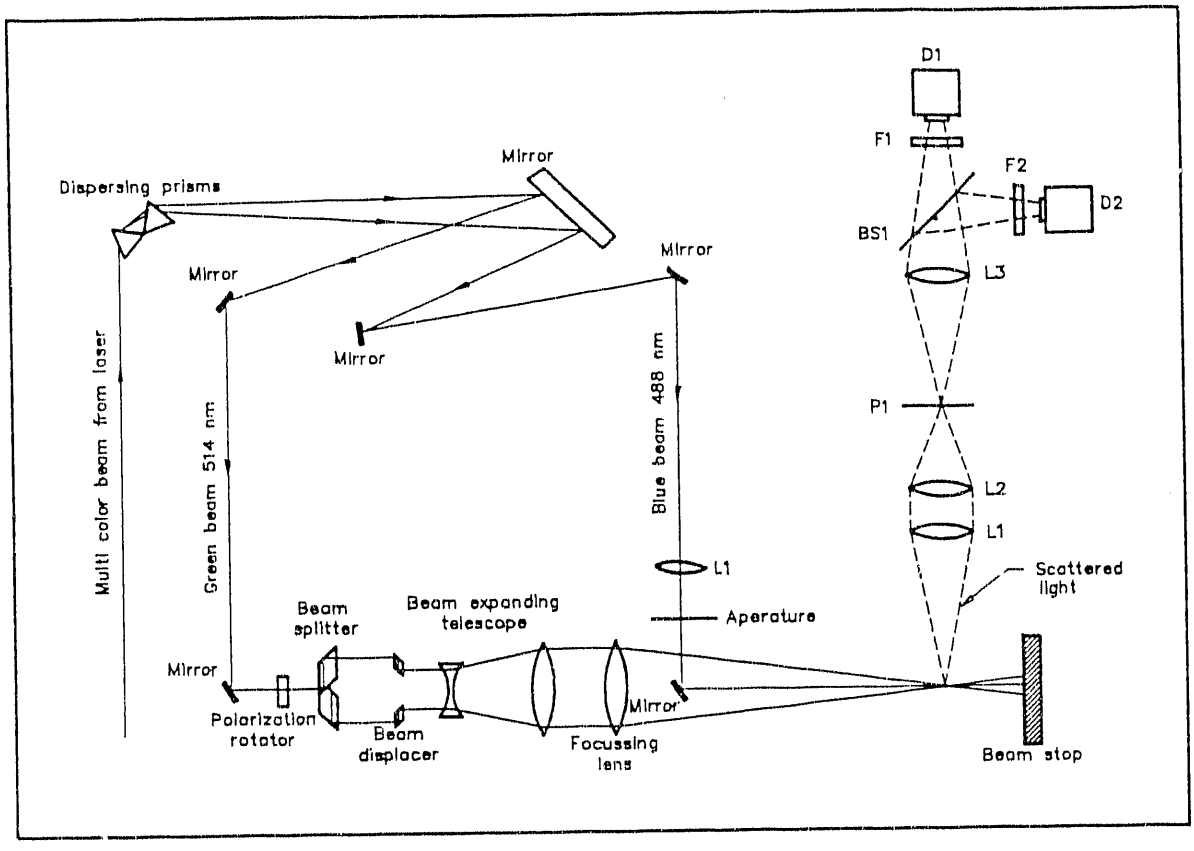

Figure 2 - Schematic of beam transmission and receiving optics indicating paths of the laser Dopler velocimeter, size measurement laser beams and collected scattered light.

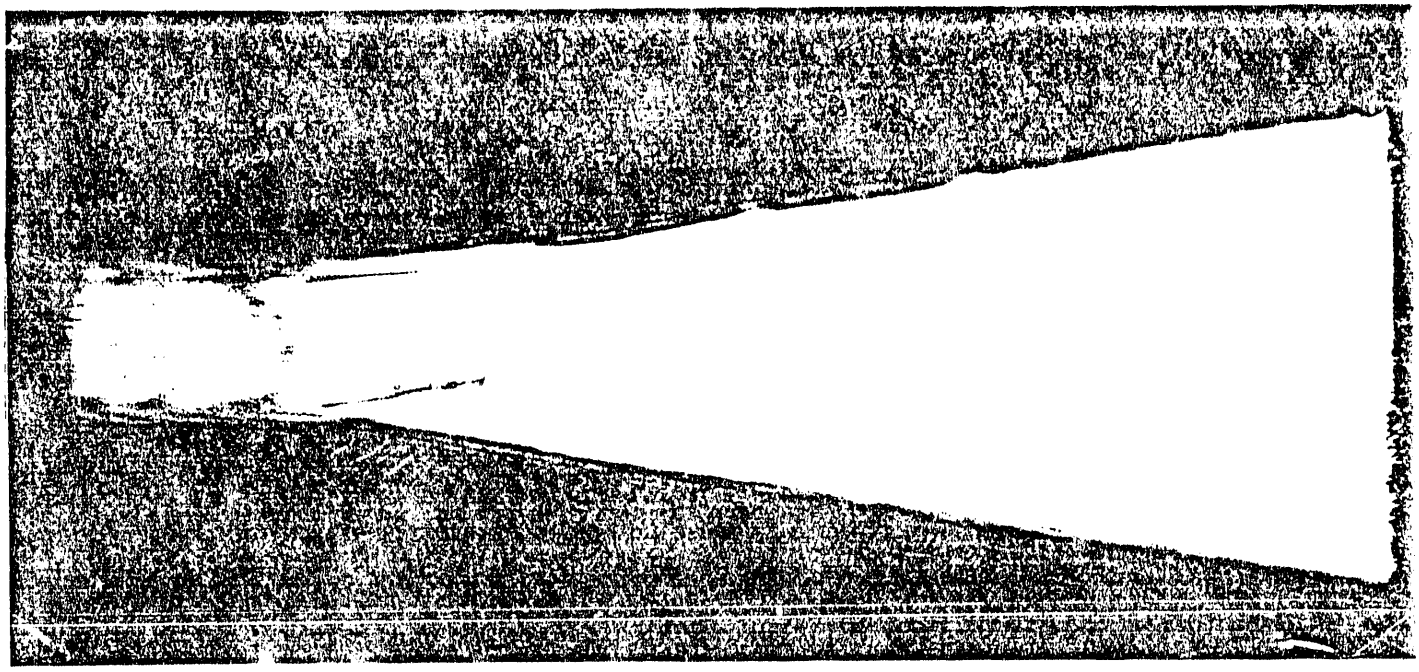

(a)

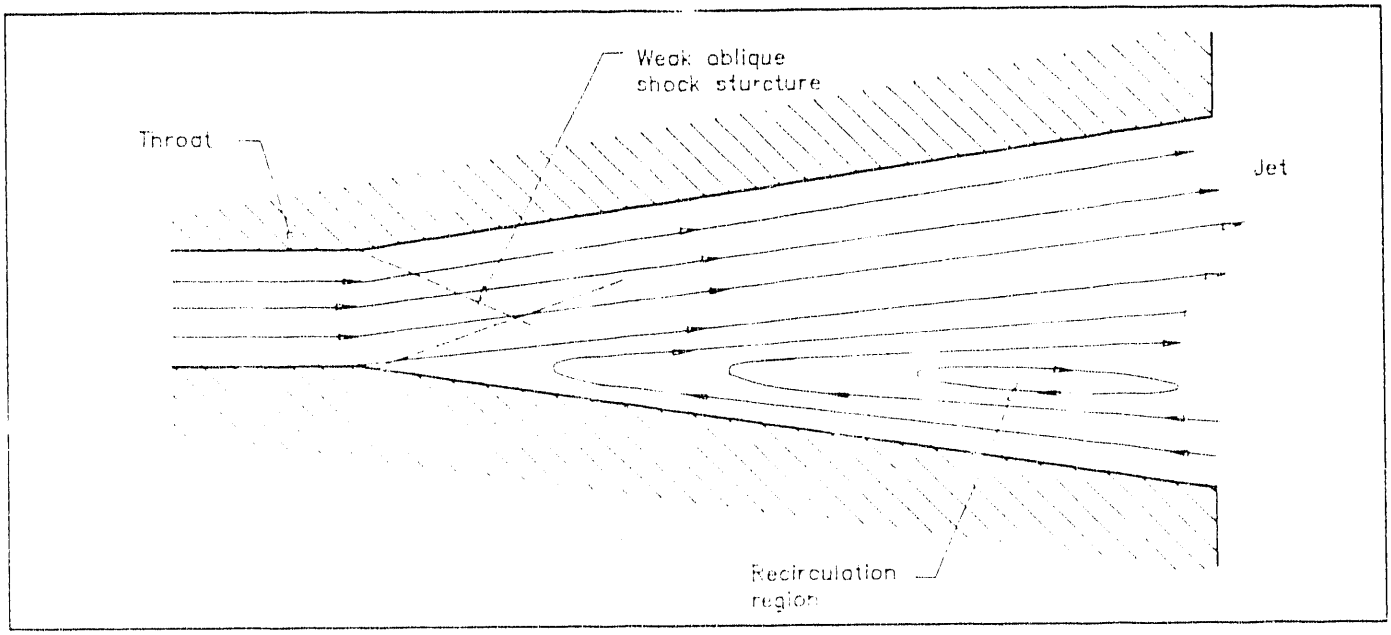

(b)

Figure 3 - (a) Schlieren photograph of oblique shock waves and (b) schematic representation of separated flow in the nozzle.

Figure 4 - Breakup of liquid tin in the throat region of the nozzle.

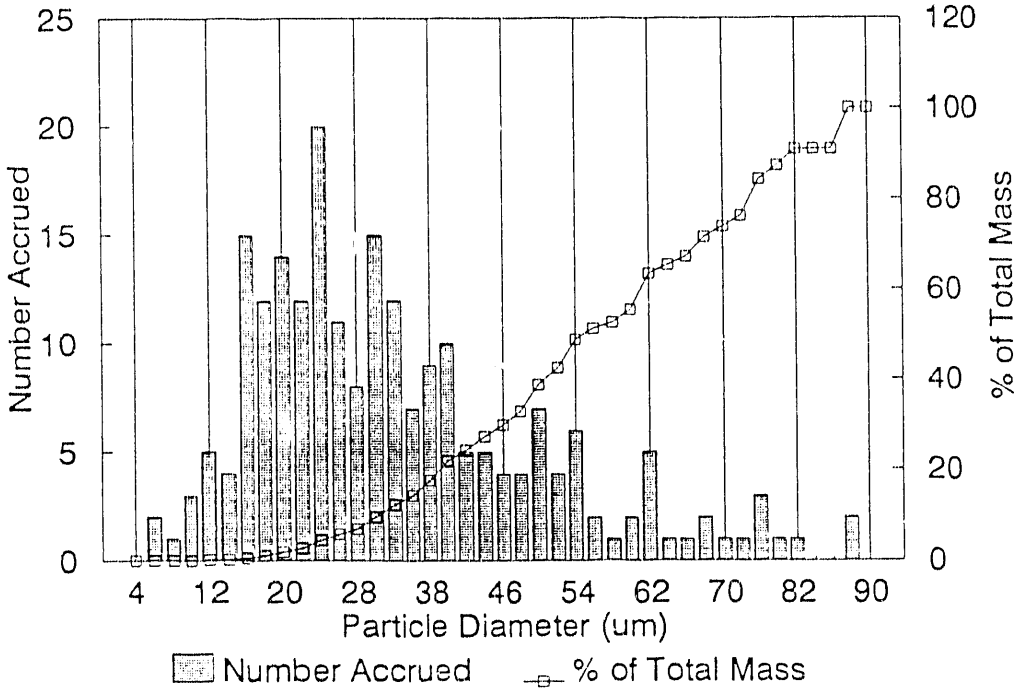

Figure 5 - Size distribution of tin particles measured in flight 10 mm from the exit of the nozzle.

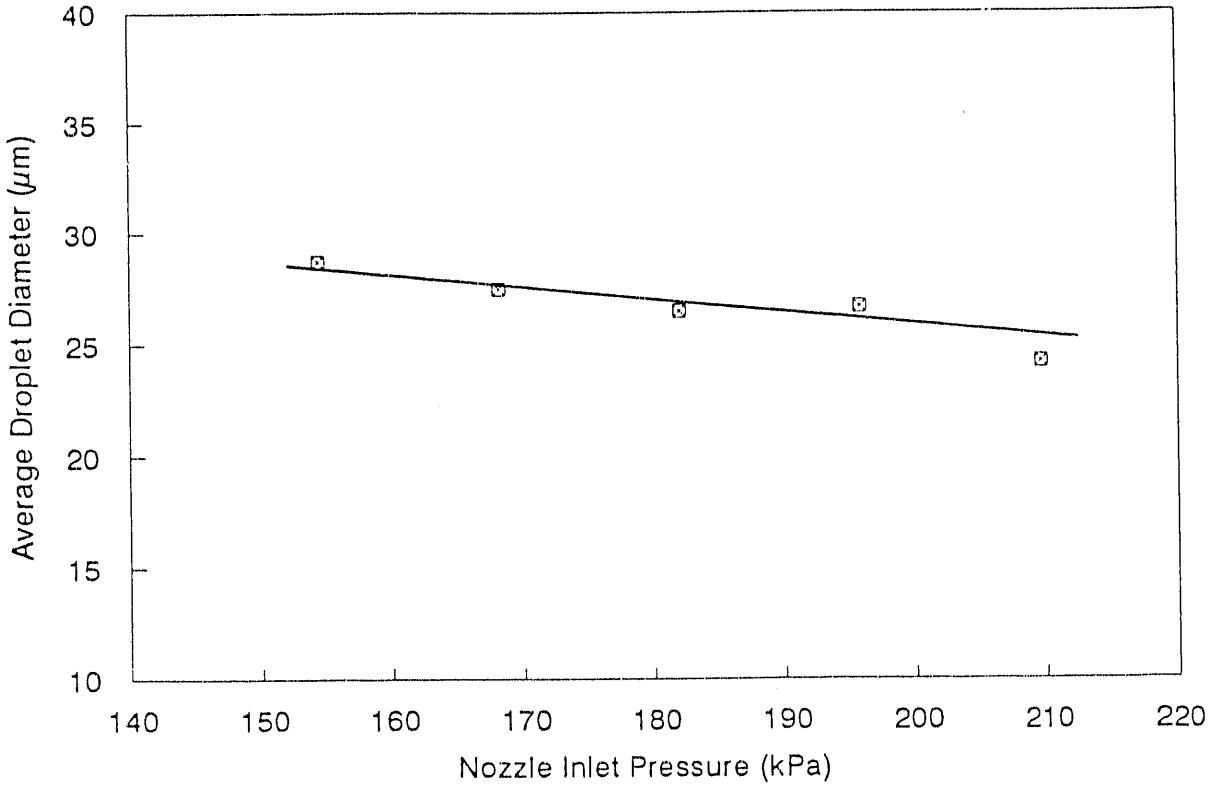

Figure 6 - Average droplet diameter as a function of nozzle inlet pressure measured 10 mm from the exit of the nozzle.

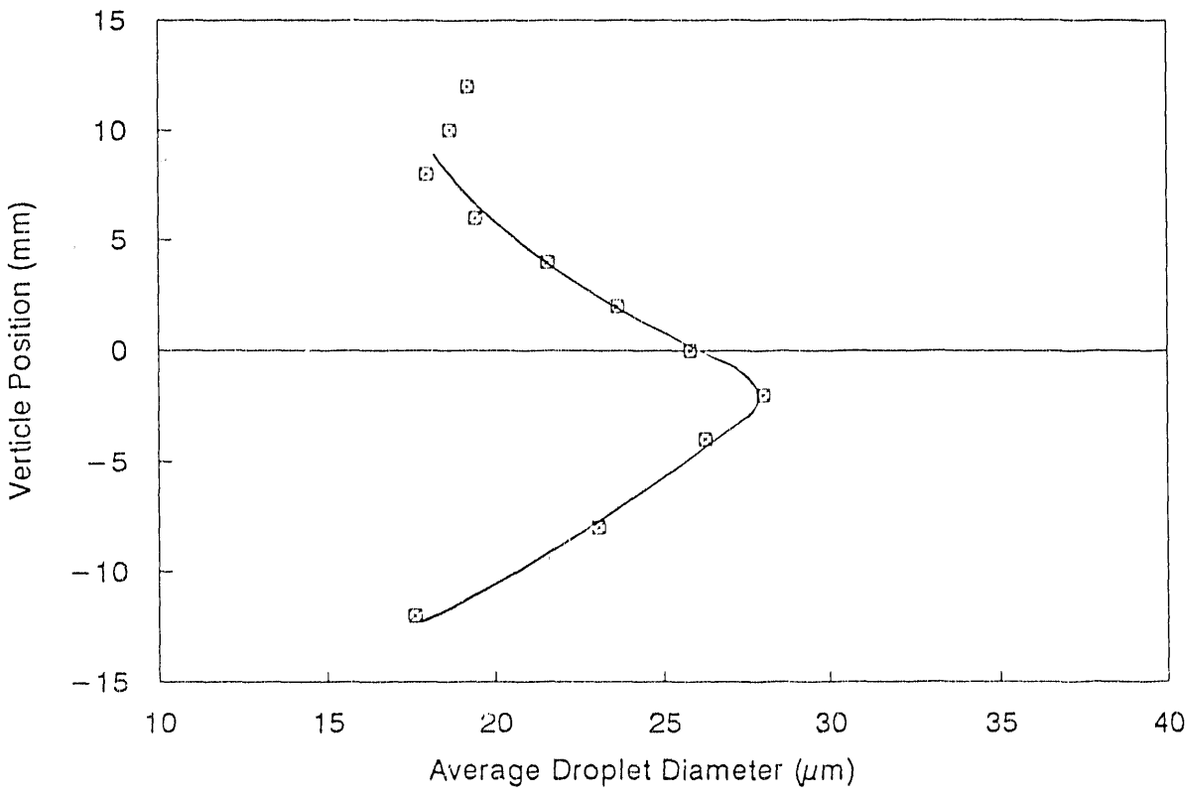

Figure 7 - Vertical spatial distribution of average droplet diameter at 10 mm from the exit of the nozzle.

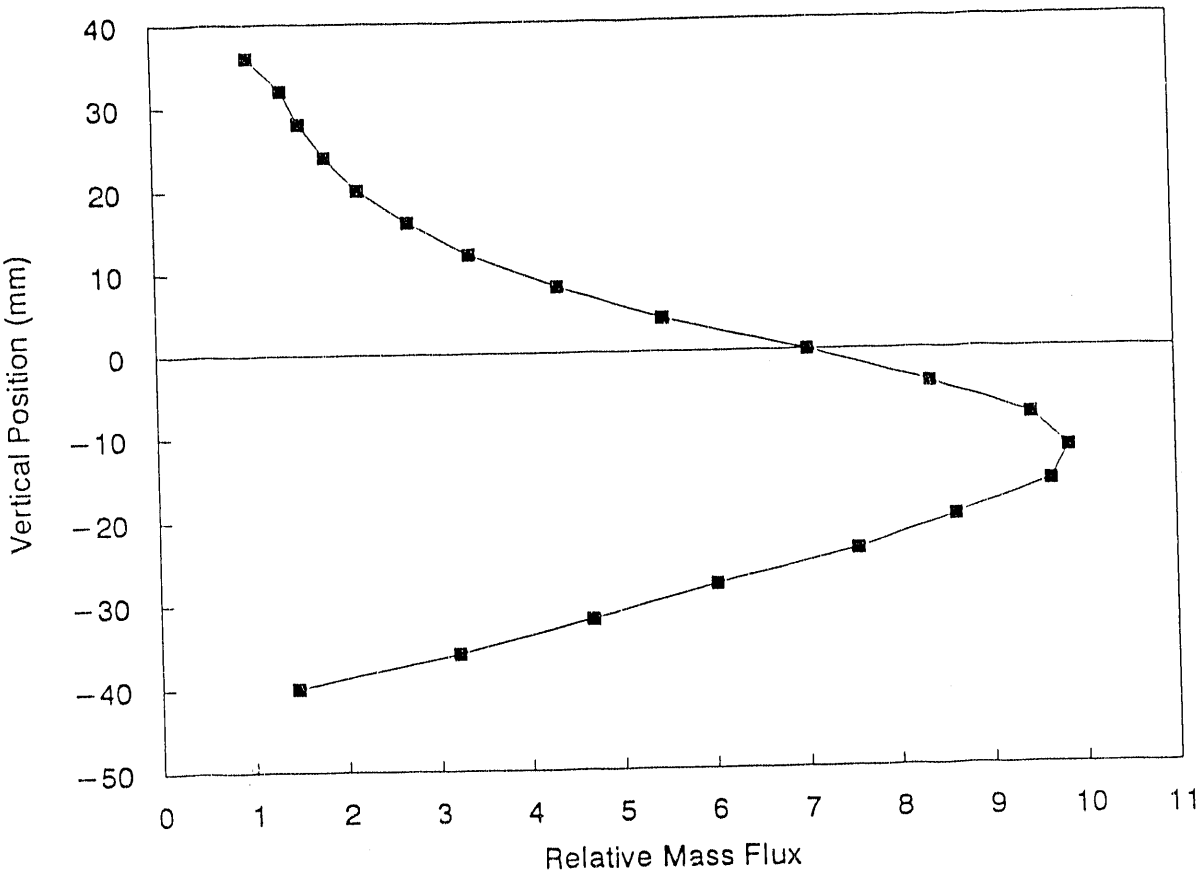

Figure 8 - Relative mass flux in the spray field.

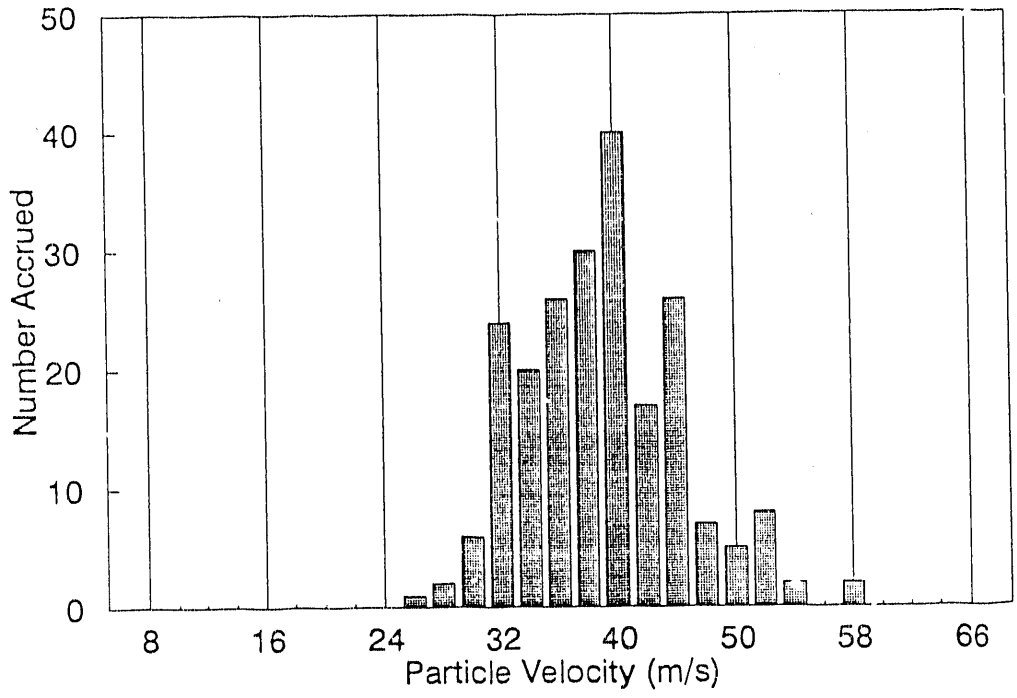

Figure 9 - Velocity distribution of particles measured in flight 10 mm from the exit of the nozzle.

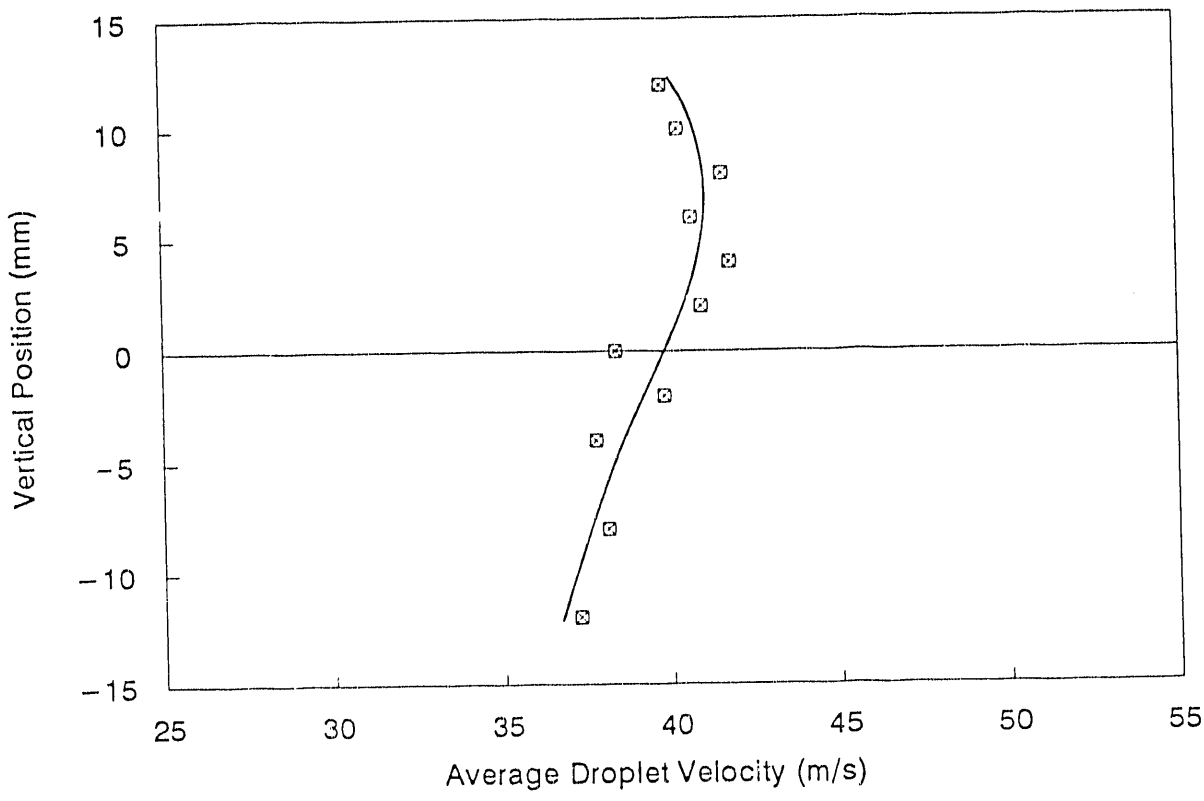

Figure 10 - Vertical spatial distribution of average particle velocity at 10 mm from the exit of the nozzle.

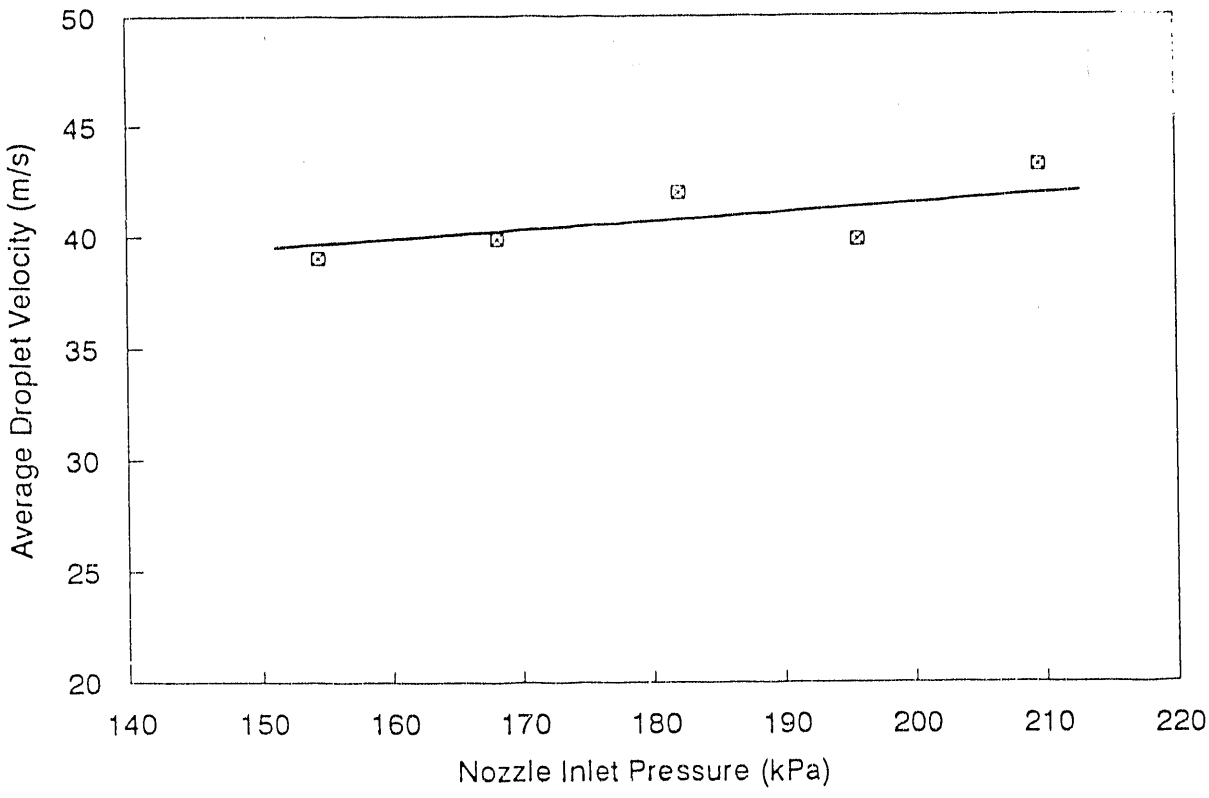

Figure 11 - Average particle velocity as a function of nozzle inlet pressure measured 10 mm from the exit of the nozzle.